

# Geophysical Research Letters®






## RESEARCH LETTER

10.1029/2023GL106879

Thi Trinh Nguyen and Li-Wei Kuo  
contributed equally to this work

## Fluid Drainage Leads to Thermal Decomposition of Wet Gouge During Experimental Seismic Slip

Thi Trinh Nguyen<sup>1</sup>, Li-Wei Kuo<sup>1,2,3</sup> , Qing-En Kong<sup>1</sup>, Chia-Wei Kuo<sup>4</sup>, Jia-Jyun Dong<sup>1,2,3</sup> ,  
Dennis Brown<sup>1,5</sup>, Huan Wang<sup>6</sup>, Szu-Ting Kuo<sup>1</sup>, Haibing Li<sup>6</sup> , and Jialiang Si<sup>6</sup>

<sup>1</sup>Department of Earth Sciences, National Central University, Taoyuan, Taiwan, <sup>2</sup>Earthquake-Disaster & Risk Evaluation and Management (E-DREaM) Center, National Central University, Taoyuan, Taiwan, <sup>3</sup>Graduate Institute of Applied Geology, National Central University, Taoyuan, Taiwan, <sup>4</sup>Science and Technology Research Institute for DE-Carbonization (STRIDE-C), National Taiwan University, Taipei, Taiwan, <sup>5</sup>Geosciences Barcelona, CSIC Barcelona, Barcelona, Spain, <sup>6</sup>MNR Key Laboratory of Deep-Earth Dynamics, Institute of Geology, Chinese Academy of Geological Sciences, Beijing, China

### Key Points:

- Thermal pressurization operates as the dynamic weakening mechanism during experimental seismic slip regardless of the ambient conditions
- Thermal pressurization ceases because of fluid drainage and is followed by kaolinite thermal decomposition
- Thermal decomposition of kaolinite tends to be initiated at large normal stresses in the seismic slip range

### Supporting Information:

Supporting Information may be found in the online version of this article.

### Correspondence to:

L. W. Kuo,  
[liweikuo@ncu.edu.tw](mailto:liweikuo@ncu.edu.tw)

### Citation:

Nguyen, T. T., Kuo, L.-W., Kong, Q.-E., Kuo, C.-W., Dong, J.-J., Brown, D., et al. (2024). Fluid drainage leads to thermal decomposition of wet gouge during experimental seismic slip. *Geophysical Research Letters*, 51, e2023GL106879. <https://doi.org/10.1029/2023GL106879>

Received 20 OCT 2023

Accepted 5 AUG 2024

### Author Contributions:

**Conceptualization:** Li-Wei Kuo

**Formal analysis:** Thi Trinh Nguyen

**Funding acquisition:** Li-Wei Kuo

**Investigation:** Thi Trinh Nguyen, Haibing Li

**Methodology:** Thi Trinh Nguyen, Jia-Jyun Dong

**Project administration:** Li-Wei Kuo

**Resources:** Huan Wang, Jialiang Si

**Software:** Qing-En Kong, Chia-Wei Kuo, Szu-Ting Kuo

**Supervision:** Li-Wei Kuo

**Abstract** Several borehole cores intersecting faults related to coseismic slip display high-temperature features, including thermal decomposition of fault gouge. We present evidence that these features may be related to fluid drainage of the slip zone during seismic slip. We sheared water-saturated kaolinite powders under both fluid drained and undrained conditions, expected for seismic slip at shallow crustal depths. Our results show typical dynamic weakening behavior regardless of conditions. Under fluid drained condition, restrengthening accompanied by the thermal decomposition of kaolinite occurs. In addition, thermal decomposition of kaolinite tends to be initiated at high normal stresses (>5 MPa) with short displacement (<5 m). We propose that thermal pressurization acts as a weakening mechanism but ceases because of fluid drainage, triggering kaolinite thermal decomposition. This finding explains seismic-slip-related clay anomalies at depth rather than at the surface, as observed in the borehole after the 1999 Mw 7.6 Chi-Chi earthquake, Taiwan.

**Plain Language Summary** Seismic faulting at depth can drive thermochemical reactions within the slip zone, given the high slip velocity and large displacement. Several slip-zone samples from deep drilling projects following catastrophic earthquakes have exhibited high-temperature geological characteristics, which were not present in fault zone outcrops hosting surface ruptures. We sheared kaolinite (as an analogue of fault zone materials) under both fluid drained and undrained conditions, simulating conditions expected during seismic slip at borehole depths. Our results show that, regardless of the applied conditions, the materials tend to weaken dramatically during shearing. However, when fluids are allowed to drain from the slip zone, there is a subsequent strengthening accompanied by the thermal decomposition of kaolinite. We suggest that thermal pressurization operates as the weakening mechanism but is ceased due to fluid drainage, resulting in the thermal decomposition of kaolinite gouges. In addition, the thermal decomposition of kaolinite tends to be triggered at large normal stresses. Because kaolinite is a common component in both fault zones and subduction zones at shallow depths, our findings have potential implications for reported thermally driven reactions within slip zones as a potential seismic indicator at shallow crustal depths.

## 1. Introduction

Dynamic fault strength (rock friction in the broad sense) and its evolution on the fault plane during an earthquake are crucial in understanding the energy partitioning of earthquakes and fault rupture dynamics (Chester et al., 2005; Scholz, 2002). Given the low thermal conductivity of rocks, the large slip rate (up to 10 m/s), and the displacement (up to tens of meters), dynamic fault strength is affected by physical and chemical processes triggered by the power density (i.e., the product of shear stress and slip velocity; Di Toro et al., 2011) released during an earthquake (e.g., frictional melting and the triggered melt lubrication mechanism; Di Toro et al., 2006). Although faulting processes (e.g., frictional melting of rocks and the associated fault lubrication) and power dissipation cannot be observed directly during an earthquake, seismic indicators (solidified frictional melts, or pseudotachylytes) have been naturally and experimentally documented (e.g., Di Toro & Pennacchioni, 2005; Sibson, 1975; Spray, 1987; Tsutsumi & Shimamoto, 1997), allowing the retrieval of key parameters related to the earthquake source (e.g., shear stress (simple shear); Di Toro et al., 2009).

© 2024. The Author(s). Geophysical Research Letters published by Wiley Periodicals LLC on behalf of American Geophysical Union.

This is an open access article under the terms of the [Creative Commons Attribution License](https://creativecommons.org/licenses/by/4.0/), which permits use, distribution and reproduction in any medium, provided the original work is properly cited.

**Validation:** Thi Trinh Nguyen, Chia-Wei Kuo, Jia-Jyun Dong, Dennis Brown  
**Visualization:** Li-Wei Kuo, Jia-Jyun Dong  
**Writing – original draft:** Thi Trinh Nguyen, Li-Wei Kuo  
**Writing – review & editing:** Li-Wei Kuo, Dennis Brown

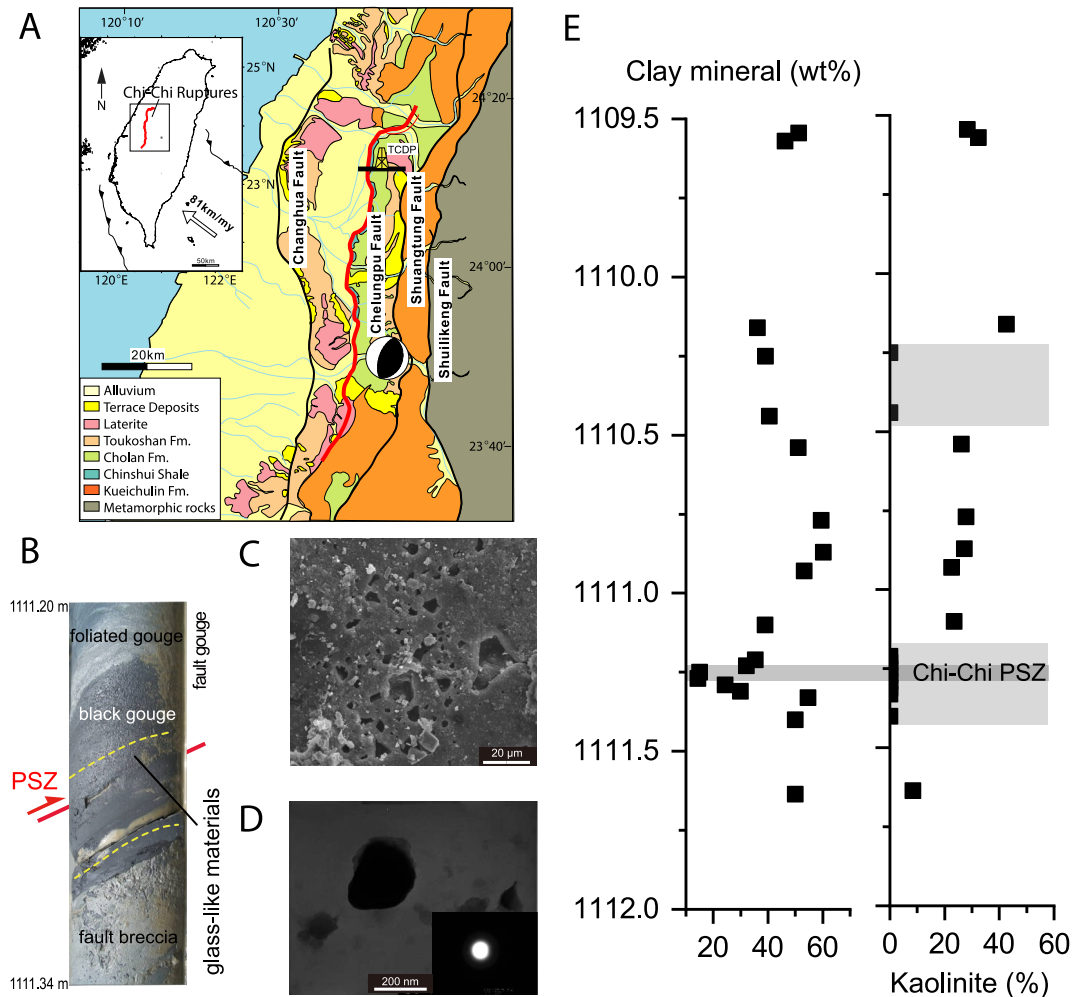


**Figure 1.** Scientific drilling projects of active faults, principal slip zone, and their microstructures and clay mineral phases (a) Geological map of the western Taiwan showing the Chelungpu fault active in the 1999 Mw7.6 Chi-Chi earthquake (in red color). The TCDP site is indicated as a yellow tower (b) Fault core composed of gray gouge and black gouges. The reported active fault zone is marked in yellow dashed lines on the core images. PSZ is marked in red within the active fault zone (c) and (d) Backscattered SEM image and TEM analysis of the PSZ samples (Kuo et al., 2011) (e) Semiquantitative weight percentage of clay minerals and kaolinite in the borehole cores. The absence of kaolinite is marked in gray rectangles.

To obtain geological features of a principal slip zone (PSZ) that could provide insights into the processes that were active during faulting, several boreholes were drilled after Mw > 7 earthquakes. These boreholes include the Wenchuan earthquake Fault Scientific Drilling project (WFSD) (Li et al., 2013) at the site of the Mw 7.9 Wenchuan earthquake, and the Taiwan Chelungpu fault Drilling Project (TCDP) (Figure 1a; Ma et al., 2006) in the Mw 7.6 Chi-Chi earthquake. In the WFSD, the PSZs at different depths were also determined to be the product of graphitization (Kuo et al., 2014) and melting processes (Wang et al., 2023), respectively, which suggest high frictional heat (>300°C) and the presence of fluids. Similarly, in the TCDP, the PSZ was the proposed cause of hot fluid-rock interaction and the demagnetization of the PSZ (temperature >350°C; Ishikawa et al., 2008; Chou et al., 2012). On the basis of thermal decomposition of kaolinite (and chlorite), Kuo et al. (2011) suggested that temperatures within the PSZ were as high as ~900–1,100°C (Figures 1b–1e).

The PSZs from both boreholes showed the effects of high temperatures and the presence of fluids. It remains unclear why high-temperature features in the PSZ were developed at depth but not at the surface (Heermance et al., 2003; Isaacs et al., 2007). In addition, current results from high-velocity rotary shear experiments have shown that high-temperature PSZs were mostly generated on room-humidity gouges, but not on wet gouges (Han et al., 2014; Kuo et al., 2017; Proctor et al., 2014). Due to the difficulty in confining fluids in the experimental

apparatus (Aretusini et al., 2021; Okuba et al., 2023), high-velocity rotary shear experiments on wet gouges were commonly conducted at low normal stresses (see the summary in Kuo et al., 2021). Using a newly developed sample holder in our experiments (Kuo et al., 2021, 2022a), we demonstrate a definitive process (the thermal decomposition of kaolinite) and the associated mechanism (from wet to dry states within principle slip zones) expected for seismic slip at shallow crustal depths. In wet kaolinite gouges, a dry state can form in the PSZ due to fluid drainage and the associated high-temperature geological features at certain normal stresses. We extrapolate our results to the TCDP (~10–20 wt% kaolinite) where the thermal decomposition of kaolinite (0 wt% kaolinite) was observed in the PSZ (Kuo et al., 2011) and provide a potential explanation for the high-temperature observations at depth rather than at the surface. Finally, we surmise that at shallow crustal depths, thermally driven reactions within gouges can be a potential seismic indicator of active faults.

## 2. Experimental Methods

Kaolinite powders were used as the starting material (Text S1 in Supporting information S1). The experiments were performed using the low to high velocity rotary shear (LHVR) apparatus equipped with a sample holder to confine water-saturated kaolinite samples (Text S1 and Figure S1 in Supporting information S1). The LHVR experiments were conducted at a normal stress of 10 MPa under either undrained (Kuo et al., 2021) or drained (Kuo, Hung, et al., 2022) conditions (Text S2 in Supporting information S1). To measure temperatures, a K-sheath thermocouple was inserted into the gouge layer ~0.5 mm below the PSZ at 2/3 of the radius of the station base (Figure S1 in Supporting information S1). A negligible volume of water was extruded from the thermocouple pinhole during compaction and shearing.

To investigate the processes responsible for fault behavior with increased slip under drained conditions, we conducted slip-stepping experiments that were stopped at approximately the maximum or minimum values of the friction coefficient. In addition, to quantify the thermal decomposition of kaolinite, which is likely to be triggered in PSZ at different depths, we conducted additional experiments at normal stresses of 2–18 MPa (Table S1 in Supporting information S1), determined the slip required for triggering kaolinite thermal decomposition, and calculated the corresponding breakdown work (i.e., the product of steady-state shear stress and slip) and power density (i.e., the product of steady-state shear stress and slip velocity; Di Toro et al., 2011).

The shear stress ( $\tau$ ) is calculated by measuring torque (Hirose & Shimamoto, 2005). The coefficient of friction ( $\mu$ ) is then calculated by dividing  $\tau$  by the normal stress ( $\sigma$ ) value (Text S3 in Supporting information S1). We consider the experimental  $\mu$  calculated in this way to be apparent because the pore fluid pressure within the PSZ was neither controlled nor measured. Because pore fluid pressure was neither controlled nor measured during the experiments, we carry out thermo-hydro-mechano-chemical modeling (Yeh et al., 2012) to estimate local pressure-temperature conditions inside the gouge layer during sliding (Text S4 in Supporting information S1). Since the sample holder contributes a constant value of intrinsic friction (Kuo et al., 2021), we have reported the experimental data without subtracting its contribution.

The experimental shearing occurred in the upper part of the gouge layer. The PSZ formed as a 100  $\mu\text{m}$  - thick in the upper part of the 2 mm thick gouge layer. Deformed samples were collected and impregnated with epoxy, cut perpendicular to the slip surface and across the diameter, and petrographic thin sections were prepared for microanalytical investigations. These include field emission electron microscopy equipped with an energy dispersive X-ray spectrometer (FESEM/EDX) and focus ion beam-transmission electron microscopy (FIB-TEM).

## 3. Results

In the undrained experiments (Figure 2a; Figure S5A in Supporting information S1),  $\mu$  increases to a peak value ( $\mu_p$ ) of ~0.28 and then decreases to a steady state value ( $\mu_{ss}$ ) of ~0.10 (an average value during steady state sliding). The measured temperature of the gouge layer increases gradually to ~300°C after ca. 4 m of slip, then almost remains constant and to a final value of ~290°C at the end of the experiment (~7 m of slip). The model shows a similar temperature evolution as that measured at the thermocouple at the same location. In addition, the model implies that pore fluid pressure within the PSZ gradually increases to ~7 MPa after <4 m of slip and sustains to the end of the experiment. The PSZ show randomly distributed smeared particles (Figure S6 in Supporting information S1), in agreement with the observation of gouge fluidization reported by Kuo et al. (2021).

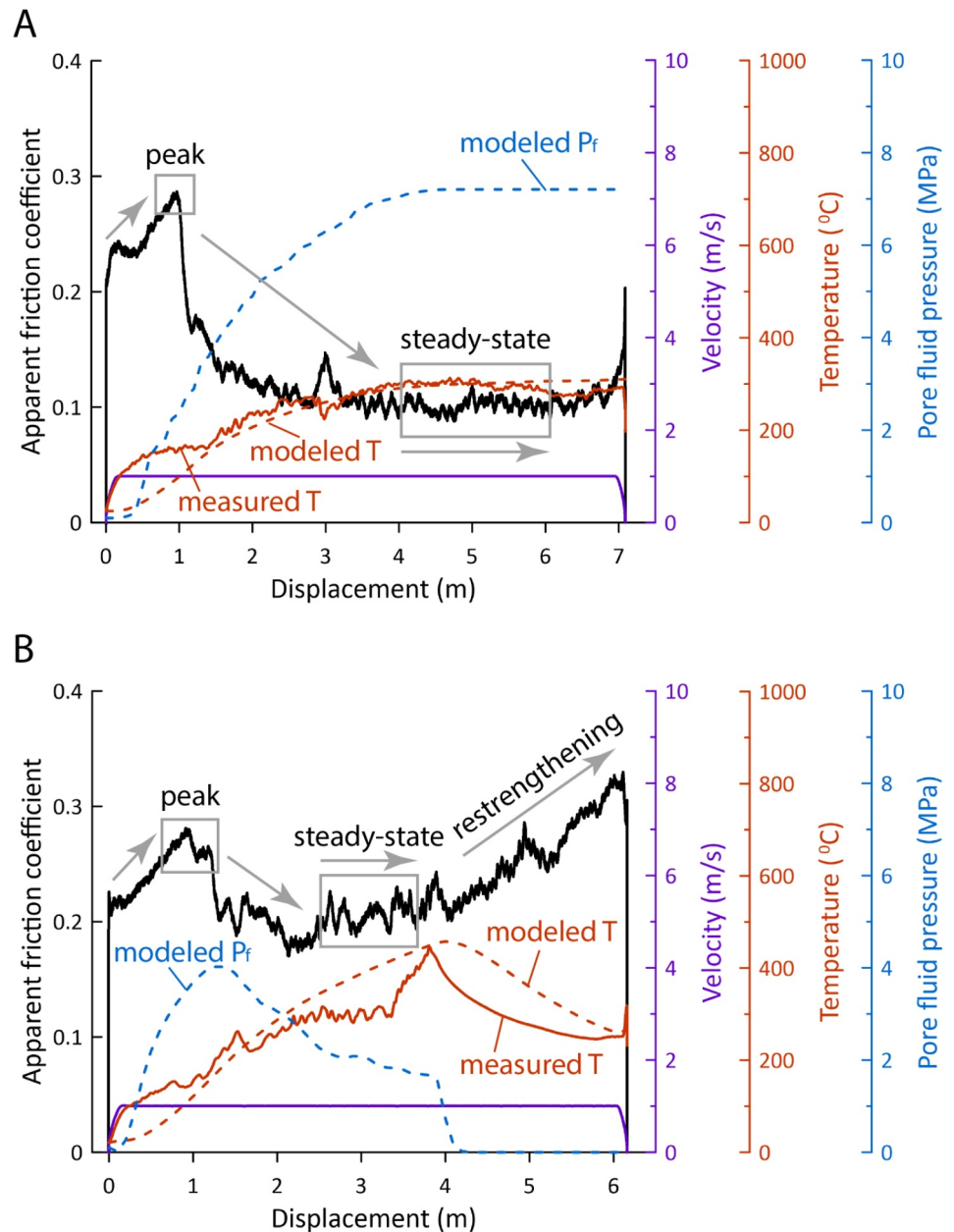


**Figure 2.** Experiments performed with LHVR on kaolinite powders at a normal stress of 10 MPa and velocity of 1 m/s. Apparent friction coefficient (shear stress/normal stress) versus displacement is shown for two experiments (see more in Figure S5 in Supporting Information S1) performed under (a) fluid undrained and (b) drained conditions. Measured temperature evolutions with displacement below the PSZ are shown in solid red lines. Modeled temperature and pore fluid pressure evolution with displacement is shown for two experiments (red dashed curves and blue dashed curves, respectively). Pore fluid pressure is modeled at the temperature measuring position.

In the drained condition experiments (Figure 2b; Figure S5B in Supporting information S1), from 0 to ca. 1 m slip,  $\mu$  increases to a  $\mu_p$  of  $\sim 0.27$  (stage I), before decreasing again to  $\mu_{ss}$  of  $\sim 0.20$  (stage II). From ca. 3.8 m of slip, at the onset of restrengthening (stage III),  $\mu$  gradually increases to ca. 0.31 at the end of sliding at  $\sim 6$  m of slip (stage IV). From the onset of slip, the temperature increases continuously to  $\sim 445^\circ\text{C}$  until the initiation of restrengthening when it rapidly decreases to a final value of  $\sim 250^\circ\text{C}$  at the end of the experiment (Figure 2b). Similarly, the modeled temperature at the thermocouple location gradually increases to  $\sim 458^\circ\text{C}$  after  $<4$  m of slip and decreases to a value of  $\sim 260^\circ\text{C}$  at the end of the experiment (Figure 2b). The similarity between measured and

modeled temperatures allows us to model the evolution of temperature and pore pressure within the PSZ and correlate them to the associated microstructures shown below.

The modeled temperature within the PSZ gradually increases to  $\sim 700^{\circ}\text{C}$  after  $<4$  m of slip ( $\sim$  at stage III), rapidly decreases to a value of  $\sim 350^{\circ}\text{C}$   $< 6$  m of slip, and then increases to  $\sim 400^{\circ}\text{C}$  at the end of the experiment (Figure 3a). Importantly, the modeled pore fluid pressure within the PSZ rapidly increases to  $\sim 4.5$  MPa after  $<1.3$  m of slip, gradually decreases to a value of  $\sim 1.6$  MPa after  $<4$  m of slip, and rapidly drops to zero at  $\sim$  the onset of restrengthening (stage III; i.e. unsaturated condition; Figure 3a). The sheared gouge becomes dryer (i.e., unsaturated condition) and its color becomes darker (Figures 3b–3e). The PSZ derived from stages I and II show numerous aggregates of sub-rounded kaolinite particles with random distributions, similar to that of the undrained condition experiments (Figures 3f and 3g; Figure S6 in Supporting information S1). Vesicles are observed in stage III as well as in stage IV with sintered textures (Figures 3h and 3i). FIB-TEM shows either a bright ring (Figure 3k) or mixed with bright spots (Figure 3l), suggesting the presence of amorphous materials and meta-kaolin within the PSZ (Figures 3j–3l). The amorphous materials may be partially induced by the gallium ion beam in the FIB system because of its strong energy (Bourdelle et al., 2012).

LHVR experiments conducted at normal stresses of 2–18 MPa under drained conditions all show restrengthening behaviors accompanied with a temperature drop and the presence of amorphous materials (Figure 4). It suggests that the triggered process determined at 10 MPa experiments also occurs at different normal stresses experiments. Therefore, it allows to recognize the onset of the triggered process (Stage IV) from the mechanical data integrated with temperature evolution (Figure 4). It is noted that slips to reach stage III at different normal stresses are varied and are plotted with power density and breakdown work (Figure 5) for further discussion.

#### 4. Discussion and Conclusion

Typical dynamic weakening behavior (Di Toro et al., 2011) is observed in both sets of experiments (Figure 2). Under water-saturated conditions, because of the small grain size of the gouge (Figure S7 in Supporting information S1), water is expected to remain within the PSZ, and this may cause shear-induced pressurization in the initial stage of slip (Faulkner et al., 2018). As slip evolves, temperatures increase to  $>300^{\circ}\text{C}$  and pore fluid pressure increases to  $\sim 4$ –7 MPa (Figure 2), allowing water to transition from fluid to vapor phase, leading to thermal expansion of water and vapourization (dilation of the gouge layer in the undrained state, Figure S5A in Supporting information S1; Chen et al., 2017), triggering thermal pressurization. Both can result in high pore pressures and the associated decrease in effective normal stress in the initial slip of experiments (e.g., Aretusini et al., 2021), as shown in the modeling (Figure 2). These are likely to be the main dynamic weakening mechanisms for undrained and drained (stage I to II) conditions (Figures 2 and 3a), consistent with the reported data (Chen et al., 2017).

In both natural and experimental examples, thermal pressurization has been shown to be a key factor in the process of clay particle rotation and movement in suspension within a gouge layer (Boullier et al., 2009; Kuo et al., 2021, 2022b). While thermal pressurization can be sustained within the gouge layer under undrained conditions (Figure 2a; Kuo et al., 2021), in drained experiments a gradual decrease in pore fluid pressure likely leads to the cessation of thermal pressurization (Figure 3a). As shearing progresses (stage II to stage III), the kaolinite powders become intensely comminuted, resulting in an increase in grain contact area. It leads to an increased shear resistance among grains and therefore to significant frictional heating at high slip rates (e.g., Kuo, Hung, et al., 2022), forming a relatively dry PSZ and high temperature at stage III. We suggest this is the main cause of the increase in temperature that initiates the thermal decomposition of kaolinite to metakaolin (from lighter to darker surface in Figures 3d and 3e; Brantut et al., 2008; Chen et al., 2013).

Our drained experiments show that the thermal decomposition of kaolinite within the slip zone during stage IV slip is accompanied by a significant temperature drop (ca.  $\sim 200^{\circ}\text{C}$ ; Figures 2b and 24). The thermal decomposition of kaolinite to amorphous metakaolin is a strong endothermic reaction (enthalpy of decomposition is  $\sim 1,000$  kJ/mol; L'vov & Ugolkov, 2005; Brantut et al., 2010; Yan et al., 2017, Figure 3k). It suggests that the observed dramatic drop in temperature that took place during stage IV slip can be interpreted to be associated with the absorption of heat during decomposition of kaolinite to metakaolin (Brantut et al., 2010), unlike the temperature plateau derived from water vapourization during shearing (enthalpy of vapourization is  $\sim 50$  kJ/mol; Chen et al., 2017). It should be noted that the thermal decomposition of kaolinite in the 2-MPa experiment occurred at a relatively lower temperature ( $\sim 200^{\circ}\text{C}$ ) than the other experiments ( $>400^{\circ}\text{C}$ ) (Figure 4). Due to the

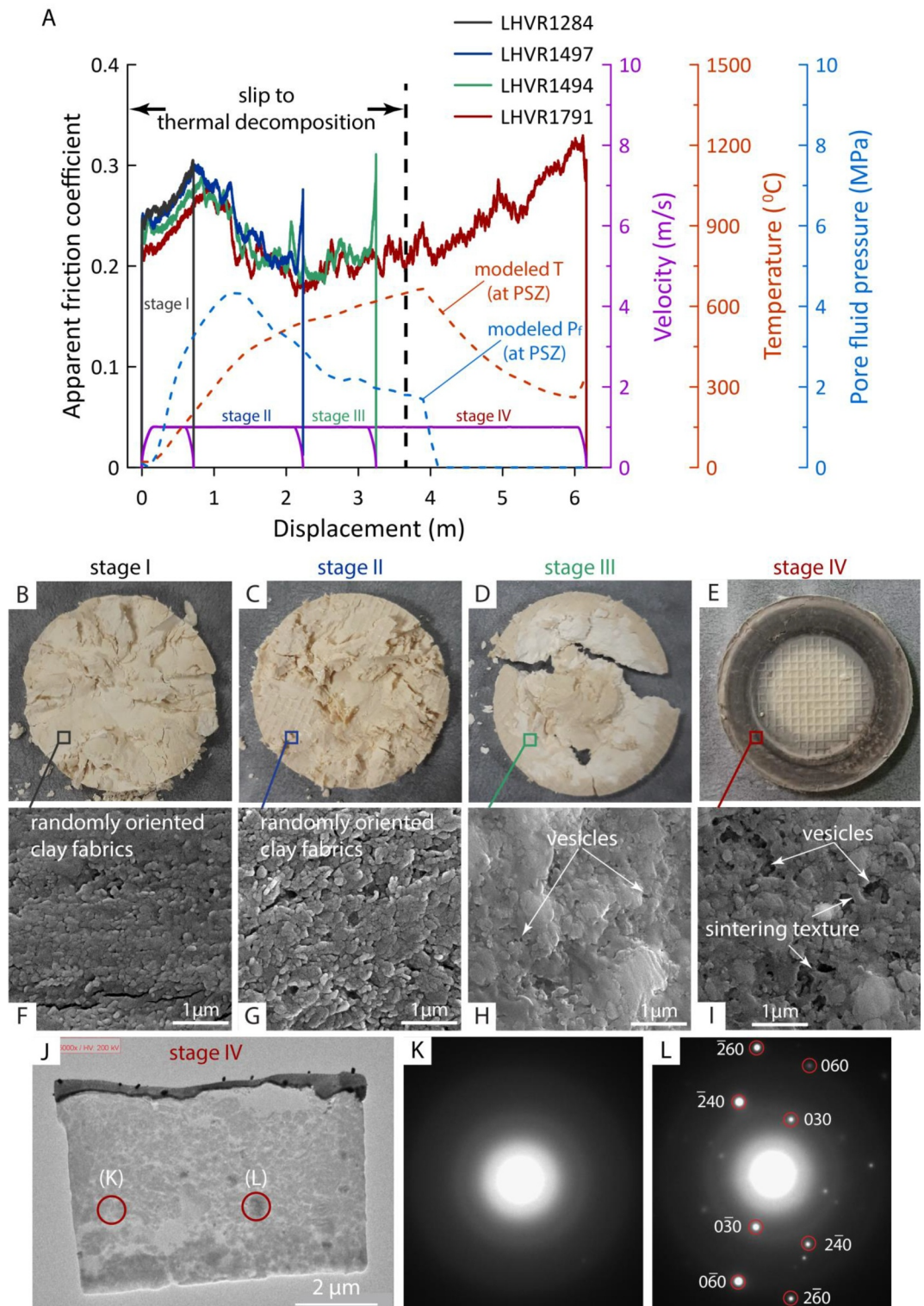


**Figure 3.** Evolution of the apparent friction coefficient, slip velocity and modeled temperature and pore fluid pressure of the PSZ with displacement of four slip-stepping experiments under drained conditions, and its microstructures at normal stress of 10 MPa and velocity of 1 m/s (a) Stage I to IV were stopped at approximately the maximum or minimum values of the friction coefficient. Stage III to IV representing slip-strengthening behavior (b)–(i) Photos of slip surface collected after individual slip-stepping experiments and the associated backscattered Field-emission SEM images of the PSZ samples (j) Field-emission SEM image of focused ion beam sample (LHVR1437, Figure S4 (b) and (k)–(l) selected area electron diffraction (SAED) pattern, showing a bright ring or mixed with bright spots.

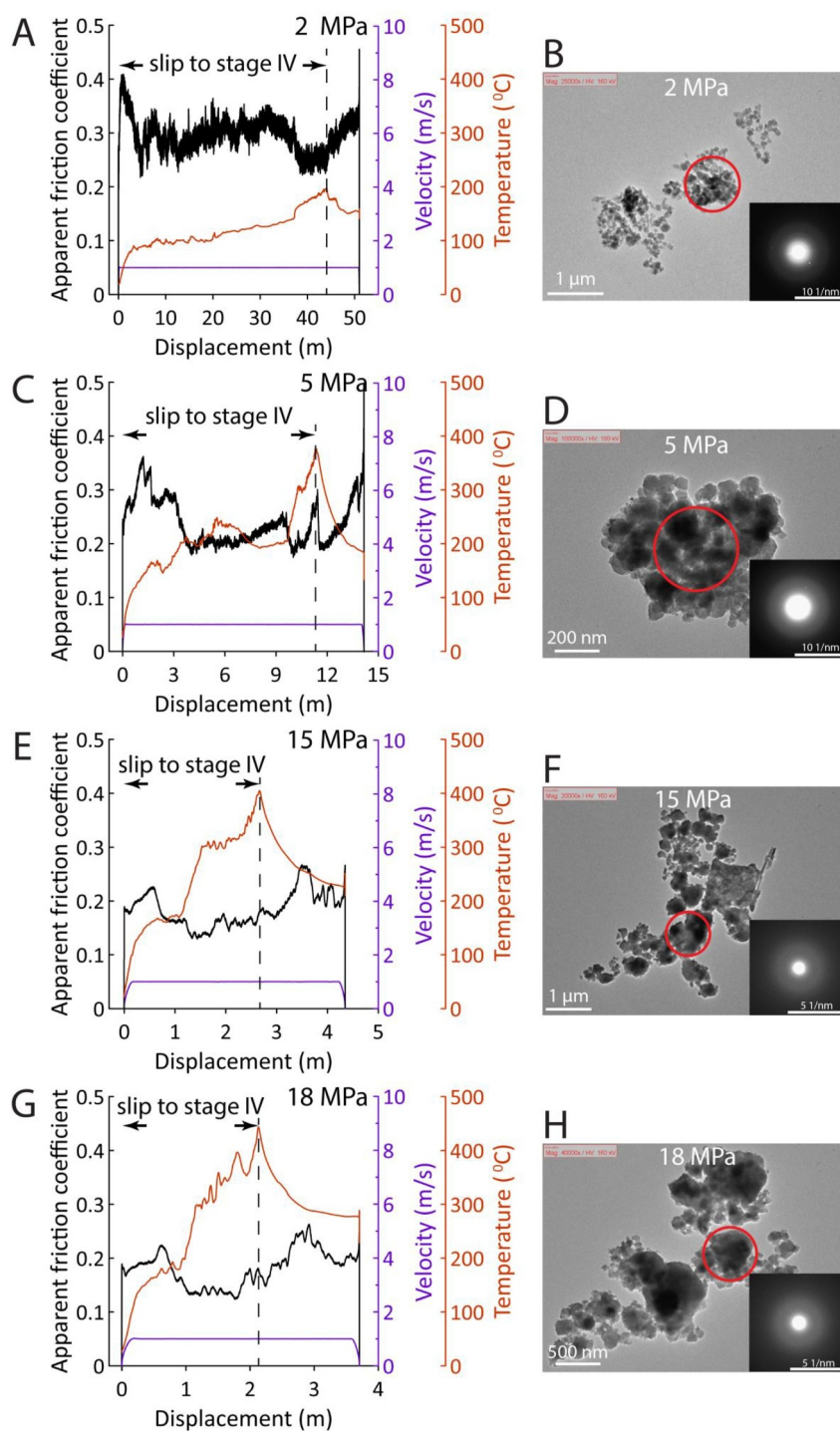


**Figure 4.** Experiments performed with LHVR on kaolinite powders at normal stresses of 2–18 MPa and velocity of 1 m/s and the associated products (a), (c), (e), (g) slip required to reach stage III (i.e., kaolinite thermal decomposition). at different normal stress (2, 5, 15, 18 MPa, respectively). The black dash line showing the estimated slip to reach stage III (b), (d), (f), (h) Micrograph photos and SAED patterns obtained from red circles of PSZs collected after the experiment showing a bright ring.

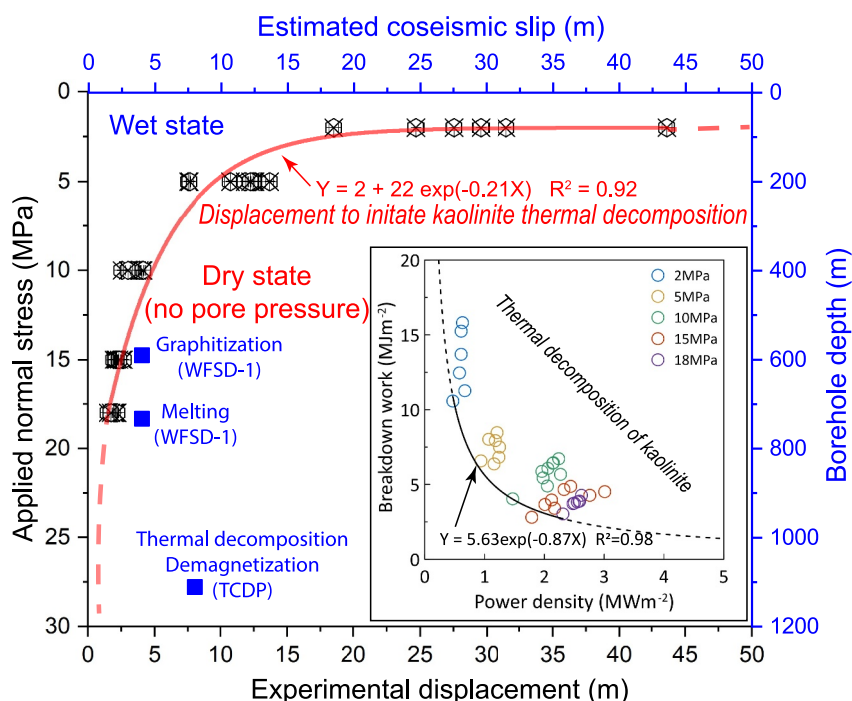


**Figure 5.** Applied normal stress versus experimental displacement required to reach initial stage III (i.e., the onset of kaolinite thermal decomposition). Borehole depth versus estimated coseismic slip for the reported drilling observation were shown in blue for comparison. Note that pore pressure is not considered in the normal stress column because the PSZ was assumed to be dry in the case. Inset showing breakdown work and power density (Di Toro et al., 2011) and marking the region of triggering thermal decomposition of kaolinite.

application of large displacements (up to 50 m) in the 2-MPa experiments, we suggest that long-term comminution induces tribochemical reactions (Hirono et al., 2014), which may allow the thermal decomposition of kaolinite to occur at lower activation energies (and thus its kinetics at a given temperature is more efficient) than thermochemical reactions (Steinike & Tkáčová, 2000).

The frictional behavior of kaolinite in our study may not be representative of natural fault zones due to their lower kaolinite content (e.g., the Chelungpu fault). Therefore, we focus on the triggering process of kaolinite shearing at seismic rates under fluid-drained conditions. The integration of the mechanical, microstructural and mineralogical observations from our experiments (the inset in Figure 5) suggests that a power density  $>0.5 \text{ MWm}^{-2}$  (for experiments performed at normal stresses  $>2 \text{ MPa}$ ) is required to trigger the thermal decomposition of kaolinite (without long-term comminution) under drained conditions. It should be emphasized that once the thermal decomposition of kaolinite is complete in a slip zone (i.e., the PSZ cannot grow further), the temperature will begin to recover due to frictional heating as the slip continues (Figure 3a), followed by a weakening behavior (Figures 4e and g).

Importantly, the slip required to reach stage III (the onset of thermal decomposition of the kaolinite) decreases exponentially with increasing normal stress (Figure 5). Since the PSZ is dry at stage III, the pore pressure is not considered in Figure 5. Considering the fact that in  $M_w > 5$  earthquakes fault displacement is typically in the range of a dozen centimeters to a few meters (Wells & Coppersmith, 1994), our results indicate that the thermal decomposition of kaolinite is triggered by  $< 5 \text{ m}$  of slip and normal stresses exceeding  $5 \text{ MPa}$  (a dry PSZ at approximately greater than  $200 \text{ m}$  depth with a rock density of  $2.5 \text{ g/m}^3$ ) under fluid-drained conditions. This finding is in agreement with previous results of rock friction experiments (Kuo et al., 2014).

Fluid drainage can occur in natural fault zones during seismic slip. For example, permeability measurements from the WFSD-1 borehole suggested the presence of coseismic fluid drainage associated with seismic rupture propagation (Xue et al., 2013). Meanwhile, microfractures and fault breccia were found below the PSZ of TCDP-A, suggesting the presence of fluid pathways (Figure 1b; Kuo et al., 2011). Therefore, we present the documented gouge graphitization/melting in WFSD (Kuo et al., 2014; Wang et al., 2023) and the observed gouge thermal

decomposition/demagnetization in TCDP (Chou et al., 2012; Kuo et al., 2011) in Figure 5, and these reported observations are broadly compatible with our research results. This implies that our findings can be applied to fault gouges with considerably low kaolinite content, which are likely to occur in both fault zones and subduction zones at shallow crustal depth (e.g., Gu et al., 2021; Kuo et al., 2011; Warr, 2022).

We suggest that, during a large earthquake, the fault gouge sheared by seismic slip under permeable conditions likely results in a relatively dry PSZ. While frictional heat continues to accumulate with increasing slip, thermochemical reactions can be triggered within the PSZ (with sufficient power density). It suggests that thermochemical reactions tend to be triggered at certain depths (i.e., large normal stress) rather than at the surface. In addition, it implies that the thermochemical reaction of fault gouge can be used as a potential indicator of active faults in the deep drilling projects, for example, thermal decomposition of kaolinite by the 1,999 Mw7.6 Chi-Chi earthquake, Taiwan (Figure 1).

## Data Availability Statement

All the experimental raw data are available in Figshare (L.-W. Kuo, 2023).

## Acknowledgments

This research was supported by the Taiwan ROC (Republic of China) National Science and Technology Council Grant NSTC 112-2628-M-008-003-MY3 and Academia Sinica Scholar Award (Grant AS-ASSA-113-01) to Li-Wei Kuo. Dennis Brown acknowledges I + D + i project PID2022-139422NB-I00 financed by MCIN/AEI/10.13039/501100011033 and by FEDER Una manera de hacer Europa.

## References

- Aretusini, S., Meneghini, F., Spagnuolo, E., Harbord, C. W., & Di Toro, G. (2021). Fluid pressurisation and earthquake propagation in the Hikurangi subduction zone. *Nature Communications*, 12(1), 248. <https://doi.org/10.1038/s41467-021-22805-w>
- Boullier, A. M., Yeh, E. C., Boutareaud, S., Song, S. R., & Tsai, C. H. (2009). Microscale anatomy of the 1999 Chi-Chi earthquake fault zone. *Geochemistry, Geophysics, Geosystems*, 10(3). <https://doi.org/10.1029/2008GC002252>
- Bourdelle, F., Parra, T., Beyssac, O., Chopin, C., & Moreau, F. (2012). Ultrathin section preparation of phyllosilicates by Focused Ion Beam milling for quantitative analysis by TEM-EDX. *Applied Clay Science*, 59, 121–130. <https://doi.org/10.1016/j.clay.2012.02.010>
- Brantut, N., Schubnel, A., Corvisier, J., & Sarout, J. (2010). Thermochemical pressurization of faults during coseismic slip. *Journal of Geophysical Research*, 115(B5). <https://doi.org/10.1029/2009JB006533>
- Brantut, N., Schubnel, A., Rouzaud, J. N., Brunet, F., & Shimamoto, T. (2008). High-velocity frictional properties of a clay-bearing fault gouge and implications for earthquake mechanics. *Journal of Geophysical Research*, 113(B10). <https://doi.org/10.1029/2007JB005551>
- Chen, J., Niemeijer, A., Yao, L., & Ma, S. (2017). Water vaporization promotes coseismic fluid pressurization and buffers temperature rise. *Geophysical Research Letters*, 44(5), 2177–2185. <https://doi.org/10.1002/2016GL071932>
- Chen, J., Yang, X., Duan, Q., Shimamoto, T., & Spiers, C. J. (2013). Importance of thermochemical pressurization in the dynamic weakening of the Longmenshan Fault during the 2008 Wenchuan earthquake: Inferences from experiments and modeling. *Journal of Geophysical Research: Solid Earth*, 118(8), 4145–4169. <https://doi.org/10.1002/jgrb.50260>
- Chester, J. S., Chester, F. M., & Kronenberg, A. K. (2005). Fracture surface energy of the Punchbowl fault, San Andreas system. *Nature*, 437(7055), 133–136. <https://doi.org/10.1038/nature03942>
- Chou, Y. M., Song, S. R., Aubourg, C., Lee, T. Q., Boullier, A. M., Song, Y. F., et al. (2012). An earthquake slip zone is a magnetic recorder. *Geology*, 40(6), 551–554. <https://doi.org/10.1130/G32864.1>
- Di Toro, G., Han, R., Hirose, T., De Paola, N., Nielsen, S., Mizoguchi, K., et al. (2011). Fault lubrication during earthquakes. *Nature*, 471(7339), 494–498. <https://doi.org/10.1038/nature09838>
- Di Toro, G., Hirose, T., Nielsen, S., Pennacchioni, G., & Shimamoto, T. (2006). Natural and experimental evidence of melt lubrication of faults during earthquakes. *Science*, 311(5761), 647–649. <https://doi.org/10.1126/science.1121012>
- Di Toro, G., & Pennacchioni, G. (2005). Fault plane processes and mesoscopic structure of a strong type seismogenic fault in tonalities (Adamello batholith, Southern Alps). *Technophysic*, 402, (1–4), 55–80. <https://doi.org/10.1016/j.tecto.2004.12.036>
- Di Toro, G., Pennacchioni, G., & Nielsen, S. (2009). Pseudotachylites and earthquake source mechanics. *International Geophysics*, 94, 87–133. [https://doi.org/10.1016/S0074-6142\(08\)00005-3](https://doi.org/10.1016/S0074-6142(08)00005-3)
- Faulker, D. R., Sanchez-Roa, C., Boulton, C., & den Hartog, S. A. M. (2018). Pore fluid pressure development in compacting fault gouge in theory, experiments, and nature. *Journal of Geophysical Research: Solid Earth*, 123, 226–241. <https://doi.org/10.1002/2017JB015130>
- Gu, D., Han, R., & Woo, S. (2021). Geological records of coseismic shear localization along the Yangsan Fault, Korea. *Journal of Geophysical Research: Solid Earth*, 126(8), e2020JB021393. <https://doi.org/10.1029/2020jb021393>
- Han, R., Hirose, T., Jeong, G. Y., Ando, J. I., & Mukoyoshi, H. (2014). Frictional melting of clayey gouge during seismic fault slip: Experimental observation and implications. *Geophysical Research Letters*, 41(15), 5457–5466. <https://doi.org/10.1002/2014GL061246>
- Heermance, R., Shipton, Z. K., & Evans, J. P. (2003). Fault structure control on fault slip and ground motion during the 1999 rupture of the Chelungpu fault, Taiwan. *Bulletin of the Seismological Society of America*, 93(3), 1034–1050. <https://doi.org/10.1785/0120010230>
- Hirono, T., Kameda, J., Kanda, H., Tanikawa, W., & Ishikawa, T. (2014). Mineral assemblage anomalies in the slip zone of the 1999 Taiwan Chi-Chi earthquake: Ultrafine particles preserved only in the latest slip zone. *Geophysical Research Letters*, 41(9), 3052–3059. <https://doi.org/10.1002/2014GL059805>
- Hirose, T., & Shimamoto, T. (2005). Growth of molten zone as a mechanism of slip weakening of simulated faults in gabbro during frictional melting. *Journal of Geophysical Research*, 110(B5). <https://doi.org/10.1029/2004JB003207>
- Isaacs, A. J., Evans, J. P., Sheng-Rong, S., & Kolesar, P. T. (2007). Structural, mineralogical, and geochemical characterization of the Chelungpu thrust fault, Taiwan. *TAO: Terrestrial, Atmospheric and Oceanic Sciences*, 18(2), 183. [https://doi.org/10.3319/tao.2007.18.2.183\(tcdp\)](https://doi.org/10.3319/tao.2007.18.2.183(tcdp))
- Ishikawa, T., Tanimizu, M., Nagaishi, K., Matsuoka, J., Tadai, O., Sakaguchi, M., et al. (2008). Coseismic fluid–rock interactions at high temperatures in the Chelungpu fault. *Nature Geoscience*, 1(10), 679–683. <https://doi.org/10.1038/ngeo308>
- Kuo, L. W. (2023). 2023-GRL-Nguyen. [Dataset]. Figshare. <https://doi.org/10.6084/m9.figshare.24412054.v1>
- Kuo, L. W., Di Felice, F., Spagnuolo, E., Di Toro, G., Song, S. R., Aretusini, S., et al. (2017). Fault gouge graphitization as evidence of past seismic slip. *Geology*, 45(11), 979–982. <https://doi.org/10.1130/G39295.1>

- Kuo, L. W., Hung, C. C., Li, H., Aretusini, S., Chen, J., Di Toro, G., et al. (2022). Frictional properties of the longmenshan fault belt gouges from WFSD-3 and implications for earthquake rupture propagation. *Journal of Geophysical Research: Solid Earth*, 127(5). <https://doi.org/10.1029/2022jb024081>
- Kuo, L. W., Li, H., Smith, S. A., Di Toro, G., Suppe, J., Song, S. R., et al. (2014). Gouge graphitization and dynamic fault weakening during the 2008 Mw 7.9 Wenchuan earthquake. *Geology*, 42(1), 47–50. <https://doi.org/10.1130/G34862.1>
- Kuo, L. W., Sone, H., Luzin, V., Yeh, E. C., Hsu, Y. J., & Tan, E. (2022b). Gouge fabrics reset by thermal pressurization record stress on faults after earthquakes. *Geology*, 50(9), 1033–1037. <https://doi.org/10.1130/G50217.1>
- Kuo, L. W., Song, S. R., Huang, L., Yeh, E. C., & Chen, H. F. (2011). Temperature estimates of coseismic heating in clay-rich fault gouges, the Chelungpu fault zones, Taiwan. *Tectonophysics*, 502(3–4), 315–327. <https://doi.org/10.1016/j.tecto.2011.02.001>
- Kuo, L. W., Wu, W. J., Kuo, C. W., Smith, S. A., Lin, W. T., Wu, W. H., & Huang, Y. H. (2021). Frictional strength and fluidization of water-saturated kaolinite gouges at seismic slip velocities. *Journal of Structural Geology*, 150, 104419. <https://doi.org/10.1016/j.jsg.2021.104419>
- Li, H., Wang, H., Xu, Z., Si, J., Pei, J., Li, T., et al. (2013). Characteristics of the fault-related rocks, fault zones and the principal slip zone in the Wenchuan earthquake Fault Scientific drilling project Hole-1 (WFSD-1). *Tectonophysics*, 584, 23–42. <https://doi.org/10.1016/j.tecto.2012.08.021>
- L'vov, B. V., & Ugolkov, V. L. (2005). Kinetics and mechanism of dehydration of kaolinite, muscovite and talc analyzed thermogravimetrically by the third-law method. *Journal of Thermal Analysis and Calorimetry*, 82(1), 15–22. <https://doi.org/10.1007/s10973-005-0886-0>
- Ma, K. F., Tanaka, H., Song, S. R., Wang, C. Y., Hung, J. H., Tsai, Y. B., et al. (2006). Slip zone and energetics of a large earthquake from the Taiwan Chelungpu-fault Drilling project. *Nature*, 444(7118), 473–476. <https://doi.org/10.1038/nature05253>
- Okuda, H., Hirose, T., & Yamaguchi, A. (2023). Potential role of volcanic glass-smectite mixtures in slow earthquakes in shallow subduction zones: Insights from low-to high-velocity friction experiments. *Journal of Geophysical Research: Solid Earth*, 128(8), e2022JB026156. <https://doi.org/10.1029/2022JB026156>
- Proctor, B. P., Mitchell, T. M., Hirth, G., Goldsby, D., Zorzi, F., Platt, J. D., & Di Toro, G. (2014). Dynamic weakening of serpentinite gouges and bare surfaces at seismic slip rates. *Journal of Geophysical Research: Solid Earth*, 119(11), 8107–8131. <https://doi.org/10.1002/2014JB011057>
- Scholz, C. H. (2002). *The mechanics of earthquakes and faulting*. Cambridge University Press. <https://doi.org/10.1017/CBO9780511818516>
- Sibson, R. H. (1975). Generation of pseudotachylite by ancient seismic faulting. *Geophysical Journal International*, 43(3), 775–794. <https://doi.org/10.1111/j.1365-246X.1975.tb06195.x>
- Spray, J. G. (1987). Artificial generation of pseudotachylite using friction welding apparatus: Simulation of melting on a fault plane. *Journal of Structural Geology*, 9(1), 49–60. [https://doi.org/10.1016/0191-8141\(87\)90043-5](https://doi.org/10.1016/0191-8141(87)90043-5)
- Steinike, U., & Tkáčová, K. (2000). Mechanochemistry of solids—Real structure and reactivity. *Journal of Materials Synthesis and Processing*, 8(3/4), 197–203. <https://doi.org/10.1023/A:1011364110355>
- Tsutsumi, A., & Shimamoto, T. (1997). High-velocity frictional properties of gabbro. *Geophysical Research Letters*, 24(6), 699–702. <https://doi.org/10.1029/97GL00503>
- Wang, H., Li, H. B., Di Toro, G., Kuo, L. W., Spagnuolo, E., Aretusini, S., et al. (2023). Melting of fault gouge at shallow depth during the 2008 MW 7.9 Wenchuan earthquake, China. *Geology*, 51(4), 345–350. <https://doi.org/10.1130/G50810.1>
- Warr, L. N. (2022). Earth's clay mineral inventory and its climate interaction: A quantitative assessment. *Earth-Science Reviews*, 234, 104198. <https://doi.org/10.1016/j.earscirev.2022.104198>
- Wells, D. L., & Coppersmith, K. J. (1994). New empirical relationships among magnitude, rupture length, rupture width, rupture area, and surface displacement. *Bulletin of the Seismological Society of America*, 84(4), 974–1002. <https://doi.org/10.1785/BSSA0840040974>
- Xue, L., Li, H. B., Brodsky, E. E., Xu, Z. Q., Kano, Y., Wang, H., et al. (2013). Continuous permeability measurements record healing inside the Wenchuan earthquake fault zone. *Science*, 340(6140), 1555–1559. <https://doi.org/10.1126/science.1237237>
- Yan, K., Guo, Y., Fang, L., Cui, L., Cheng, F., & Li, T. (2017). Decomposition and phase transformation mechanism of kaolinite calcined with sodium carbonate. *Applied Clay Science*, 147, 90–96. <https://doi.org/10.1016/j.clay.2017.07.010>
- Yeh, G. T., Tripathi, V. S., Gwo, J., Cheng, H., Cheng, J., Salvage, K., & Siegel, M. D. (2012). Hydrogeochem: A coupled model of variably saturated flow, thermal transport, and reactive biogeochemical transport. *Groundwater React Transp Models*, 3–41. <https://doi.org/10.2174/978160805306311201010003>